pathway at lower pH. This is apparent in the virtually linear dependence of $1/\tau$ upon pH between pH 6 and 8 (Figure 2b).

The large k_f and k_{eff} rate constants, which we calculate for HONi(ATP) + bpy (step 1-2 in Scheme II), indicate that the hydroxo ligand labilizes k_w and the Ni(II) + N-7 adenosine interaction in HONi(ATP). The increase of k_f could also be explained in part by an increase in K_{stk} for HONi(bpy).

If bpy is bound outer sphere in the HONi(ATP)(bpy) complex, then steps 4 and 5 in Scheme III would not be applicable and the formation rate would be independent of the rate of water dissociation. This could account for the large increase of k_f for HONi(ATP)(bpy) relative to k_f for Ni(ATP)(bpy).

In the absence of other information, Scheme III is preferred for HONi(ATP) + bpy because it is consistent with the variations of all three ternary rate constants. Furthermore, there is some precedent (from binary trivalent metal complexes)[49,50] for rate constant increases of the magnitude calculated by eq 5 for the hydroxo ternary complex (see k_{eff} in Table IV).

Conclusions

We have examined the formation kinetics of the Ni(II) + bpy and Ni|ATP + bpy systems and found that each exhibits one relaxation effect. The rate constant of the former is within a factor of 2 of the value predicted if the RDS is water dissociation. This reduction of k_f is consistent with a small involvement of the chelation ring-closure step in the RDS.

The ternary relaxation rate increases nearly linearly with increasing pH over our entire pH range. We have quantitatively modeled this behavior with a mechanism that includes three parallel ternary formation steps, which differ by the degree of protonation.

We conclude that charge donation from the hydroxo ligand, and to a lesser extent from the phosphate groups of ATP, results in a labilization of the remaining metal-bound water molecules and thus increases the forward rate constant. This trend dominates all other variations within this series of reactions. A secondary trend may be due to an interaction prior to the dissociation of water from the binary complex (the RDS) in which bpy stacks with ATP but is not bound to the metal ion. The stability of this interaction appears to be enhanced in HONi(ATP) + bpy and decreased in Ni(ATPH) + bpy relative to Ni(ATP) + bpy.

This is one of a small number of investigations that have studied the kinetics of ternary systems over a wide range of conditions. The collection of data over a wide range of pH has allowed ternary protonated and hydroxylated pathways for the Ni|ATP|bpy system to be characterized for the first time.

Acknowledgment. This work was supported by the NIH in the form of a research grant to J.E.S. (GM-13,116). We thank Dr. Ronald Nohr (Kimberly-Clark, Inc., Atlanta, GA) for his assistance in the early stages of data modeling and Dr. Helmut Sigel (Institute for Inorganic Chemistry, University of Basel, Basel, Switzerland) for helpful comments and the donation of software that proved useful in the ternary equilibrium calculations.

Registry No. ATP, 56-65-5; bpy, 366-18-7; Ni, 7440-02-0.

(49) Gouger, S.; Stuehr, J. *Inorg. Chem.* **1974**, *13*, 379-84.
(50) Miceli, J.; Stuehr, J. *J. Am. Chem. Soc.* **1968**, *90*, 6967-72.
(51) Bechtold, D. B.; Liu, G.; Dodgen, H. W.; Hunt, J. P. *J. Phys. Chem.* **1978**, *82*, 333-7.

Contribution from the Department of Chemistry, Princeton University, Princeton, New Jersey 08544, and Department of Biochemistry, University of Georgia, Athens, Georgia 30602

Resonance Raman Spectra of Rubredoxin: New Assignments and Vibrational Coupling Mechanism from Iron-54/Iron-56 Isotope Shifts and Variable-Wavelength Excitation

Roman S. Czernuszewicz,† Jean LeGall,‡ Isabel Moura,‡ and Thomas G. Spiro*†

Received September 24, 1985

Resonance Raman spectra are reported for rubredoxin from *Desulfovibrio gigas* in frozen solution (77 K) with excitation by several lines of Ar^+ and Kr^+ lasers, from 488.0 to 568.2 nm. The use of low-temperature and variable-wavelength excitation has provided more complete spectra than were hitherto available, and several new bands are reported. All three components of the $\nu_3(T_2)$ asymmetric Fe-S stretching mode of the FeS_4 tetrahedron have been identified with the aid of ^{54}Fe substitution, at 376, 366, and 348 cm^{-1}. The isotope shifts, 1.1-2.5 cm^{-1}, are smaller than expected for the asymmetric vibrations and reveal that the component modes are vibrationally coupled to other modes of the cysteine ligands, most probably involving SCC bending. The previous assignment of one of the ν_3 components to a band at 324 cm^{-1} is excluded by its lack of isotope shift; most likely this band contains one or more of the coupled SCC modes. Numerous overtone and combination bands of the Fe-S stretches are observed, and a band at 653 cm^{-1} is assigned to a C-S stretching mode. The $\nu_2(E)$ and $\nu_4(T_2)$ SFeS bending modes are located at 130 and 150 cm^{-1}. The ν_2 band is enhanced with 4965-Å excitation, and its intensity is suggested to arise via its A_1 component in the effective optical symmetry, D_{2d}, of the chromophore. In contrast, the ν_4 mode is enhanced at 5682 Å, and it appears to be depolarized; a vibronic enhancement mechanism is suggested whereby the E component of this mode mixes the locally resonant $^6B_2$ charge-transfer excited state with the nearby ^6E state. A similar intensity variation of the ν_3 components suggests that the 376-cm^{-1} band represents the asymmetric Fe-S stretch oriented along the D_{2d} symmetry axis, while the other two bands arise from the perpendicular vibrations.

Introduction

Rubredoxin is the simplest member of the iron-sulfur proteins,[1] containing a single high-spin Fe^{III} ion, which undergoes reversible one-electron reduction at a potential close to -0.05 V.[2] The X-ray crystal structure of oxidized protein from *Clostridium pasteurianum* has been determined to a resolution of 1.2 Å.[3] The Fe^{III} ion is coordinated by four cysteine side chains, in a tetrahedral arrangement. Although one of the Fe-S bonds was initially found to be anomalously short,[4] subsequent refinement has removed the anomaly; all of the Fe-S distances are within experimental error of the mean value, 2.29 Å. The Fe-K edge EXAFS spectrum[5]

* To whom correspondence should be addressed.
† Princeton University.
‡ University of Georgia.

(1) Spiro, T. G., Ed. "Iron-Sulfur Proteins"; Wiley-Interscience: New York, 1982.
(2) Eaton, W. A.; Lovenberg, W. In "Iron-Sulfur Proteins"; Lovenberg, W., Ed.; Academic Press: New York, 1973; Vol. 2, Chapter 3.
(3) Watenpaugh, K. D.; Sieker, L. C.; Jensen, L. H. *J. Mol. Biol.* **1979**, *131*, 509-522.
(4) Watenpauch, K. D.; Sieker, L. C.; Herriott, J. R.; Jensen, . H. *Acta Crystallogr., Sect. B: Structur. Crystallogr. Cryst. Chem.* **1973**, *29B*, 943-956.

0020-1669/86/1325-0696$01.50/0

is superimposable on that of the synthetic analogue complex[6] $Fe(S_2\text{-}o\text{-}xyl)_2^-$ (S_2-o-xyl = o-xylene-α,α'-dithiolate), which has essentially equal Fe–S bonds of average length 2.267 Å. While the active site of the protein contains a simple FeS_4 coordination tetrahedron, its spectroscopic characteristics are decidedly nontetrahedral. Thus single-crystal optical spectroscopy[2] has shown the first S → Fe charge-transfer electronic transition to be split into tetragonal components, which are separated by 2500 cm^{-1}, and the EPR spectrum[7] is completely rhombic, with $D = 1.76$ cm^{-1} and $E = 0.485$ cm^{-1}. Although the resonance Raman (RR) spectrum was initially analyzed[8] in terms of tetrahedral assignments, subsequent reexamination showed the RR spectrum of rubredoxin,[9,10] as well as of $Fe(S_2\text{-}o\text{-}xyl)_2^-$,[10] to be nontetrahedral.[10] The major source of the symmetry lowering of the vibrational spectrum was suggested[10] to be vibrational coupling of the Fe–S stretches with SCC bending modes of the cysteine ligands, but model calculations failed to reproduce the wide splittings that were implied by the several bands observed in the Fe–S stretching region.

Because it provides a vibrational fingerprint of a chromophore and because the vibrational frequencies are sensitive to the details of local structure, RR spectroscopy is a useful monitor of biological structure and is being applied to a variety of iron–sulfur proteins.[11] To assure a reliable interpretation of the spectra, it is important to understand the origin of the bands in detail, particularly for the simplest Fe–S structure. In this work we reexamine the rubredoxin RR spectrum, using low-temperature techniques to improve resolution and variable-wavelength excitation to bring out subtle but important details. In addition, ^{54}Fe substitution has been employed to assign the Fe–S stretching vibrations definitively. A more coherent picture of the FeS_4 vibrational spectrum than has hitherto been available emerges from this work.

Experimental Section

Materials and Methods. Details concerning the isolation and purification of rubredoxin from *Desulfovibrio gigas* have been described elsewhere.[12] ^{54}Fe-substituted protein was prepared from apoprotein following the reconstitution method previously reported for desulforedoxin from *D. gigas*.[13] The electronic absorption spectrum was recorded at room temperature on a Cary Model 14 spectrophotometer.

Exciting radiation for resonance Raman spectra was provided by Coherent Radiation CR-5 Ar^+ (4880, 4965, 5145 Å) and Spectra Physics 171 Kr^+ (5208, 5309, 5682 Å) lasers. The scattered radiation was dispersed by a Spex 1401 double monochromator and detected by a cooled RCA 31034A photomultiplier tube using an Ortec 9315 photon-counting system, under the control of a MINC II (DEC) minicomputer. Spectra were recorded digitally by backscattering directly off the surface of a frozen solution kept in a liquid-N_2 Dewar.[14] Under these conditions no protein damage was observed, even during prolonged (~6–12 h) spectral data acquisition at laser power levels of ~200–400 mW. In addition, this technique eliminates interference from glass or quartz scattering, since the frozen protein solutions require no covering.[14] The protein samples (~3 mM) were in 0.05 M Tris–HCl buffer, pH 7.5. Polarization measurements were carried out on the frozen solutions[15] at each wavelength by analyzing the scattered light (180°) in front of the monochromator slit. Low-temperature difference spectra were obtained by using a tuning fork difference Raman cell, described in detail in ref 16. This device moves a divided sample cup through the focused laser beam, using the swinging motion of a spring attached to a copper cold finger, and driven at its resonance frequency (~30–40 Hz) by a solenoid and magnet. In this way two frozen samples are alternately excited and a synchronous signal is sent to gating and counting electronics to allow independent analysis of the scattered light in two channels and subsequent independent accumulation and storage of the data in a MINC II computer. To obtain a difference spectrum the resulting two independent spectra are subtracted digitally. The spectral slit width was 4 cm^{-1} and the spectrometer was advanced in 0.2-cm^{-1} increments. The signal/noise was sufficient to assure that the errors in the calculated[17a] frequency differences are no larger than 7%.

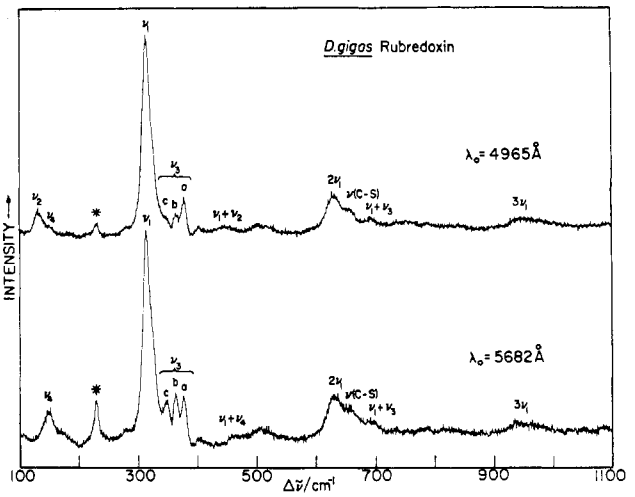

Figure 1. Resonance Raman spectra of oxidized *D. gigas* rubredoxin obtained in a liquid-N_2 Dewar with 4965-Å Ar^+ (upper trace) and 5682-Å Kr^+ (bottom trace) laser excitations and 5-cm^{-1} slit widths. For these data the spectrometer was advanced in 0.5-cm^{-1} increments.

Table I. Rubredoxin RR Frequencies and Assignments

ν, cm^{-1}	assignt[a]	ν, cm^{-1}	assignt[a]
130	δ_{SFeS},[a] ν_2,[b] $A_1(E)$[c]	403	?
		443	$\nu_1 + \nu_2$
150	δ_{SFeS}, ν_4, $E(T_2)$	463	$\nu_1 + \nu_4$
		502	?
174	δ_{FeSC}	518	?
184	δ_{FeSC}	627	$2\nu_1$
314	ν_{FeS}, ν_1, A_1	653	ν_{CS}
324	δ_{SCS}?	689	$\nu_1 + \nu_{3a}$
348	ν_{FeS}, ν_{3c}, $E(T)_2$	733	$\nu_{3a} + \nu_{3b}$
(1.1)[d]		751	$2\nu_{3a}$
363	ν_{FeS}, ν_{3b}, $E(T_2)$	757	$2\nu_1 + \nu_2$
(1.5)		777	$2\nu_1 + \nu_4$
376	ν_{FeS}, ν_{3a}, $B_2(T_2)$	940	$3\nu_1$
(2.5)			

[a] δ_{xyz} and ν_{xy} are the bending and stretching internal coordinate involving the indicated atoms. [b] ν_{1-4} are the normal modes of a XY_4 tetrahedron. [c] Symmetry designation for the $D_{2d}(T_d)$ point groups. [d] ^{54}Fe-natural abundance isotope shifts.

Results

Figure 1 shows low-temperature RR spectra for oxidized rubredoxin from *D. gigas*. The spectra are much better resolved than those reported previously[10] and reveal new features. Band frequencies and assignments are given in Table I. These spectra

(5) Shulman, R. G.; Eisenberger, P. I.; Teo, R. K.; Kincaid, J. M.; Brown, G. S. *J. Mol. Biol.* **1978**, *124*, 305–321.
(6) Lane, R. W.; Ibers, J. A.; Frankel, R. B.; Papefthymiou, G. C.; Holm, R. H. *J. Am. Chem. Soc.* **1977**, *99*, 84–98.
(7) Peisach, J.; Blumberg, W. E.; Lode, E. T.; Coon, M. J. *J. Biol. Chem.* **1971**, *246*, 5877–5881.
(8) (a) Long, T. V.; Loehr, T. M. *J. Am. Chem. Soc.* **1970**, *92*, 6384–6386. (b) Long, T. V.; Loehr, T. M.; Allkins, J. R.; Lovenberg, W. J. *J. Am. Chem. Soc.* **1971**, *93*, 1809–1811.
(9) Yamamoto, T.; Rimai, L.; Heyde, M. E.; Palmer, G., unpublished results, 1972, cited in ref 2.
(10) Yachandra, V. K.; Hare, J.; Moura, I.; Spiro, T. G. *J. Am. Chem. Soc.* **1983**, *105*, 6455–6461.
(11) (a) Yachandra, V. K.; Hare, J.; Gewirth, A.; Czernuszewicz, R. S.; Kimura, T.; Holm, R. M.; Spiro, T. G. *J. Am. Chem. Soc.* **1983**, *105*, 6462–6468. (b) Johnson, M. K.; Czernuszewicz, R. S.; Spiro, T. G.; Fee, J. A.; Sweeny, W. V. *J. Am. Chem. Soc.* **1983**, *105*, 6671–6678. (c) Johnson, M. K.; Czernuszewicz, R. S.; Spiro, T. G. *J. Biol. Chem.* **1983**, *258*, 12771–12774. (d) Johnson, M. K.; Hare, J. W.; Spiro, T. G.; Moura, J. J. G.; Xavier, A. V.; LeGall, J. *J. Biol. Chem.* **1981**, *256*, 9806–9808. (e) Johnson, M. K.; Spiro, T. G.; Mortenson, L. E. *J. Biol. Chem.* **1982**, *257*, 2447–2452.
(12) Moura, I.; Bruschi, M.; LeGall, J.; Moura, J. J. G.; Xavier, A. V. *Biochem. Biophys. Res. Commun.* **1976**, *75*, 1037–1044.
(13) Moura, I.; Huynh, B. H.; Housinger, R. P.; LeGall, J.; Xavier, A. V.; Münck, E. *J. Biol. Chem.* **1980**, *255*, 2493–2498.
(14) Czernuszewicz, R. S.; Johnson, M. K. *Appl. Spectrosc.* **1983**, *37*, 297–298.
(15) Moulis, J.-M.; Meyer, J.; Lutz, M. *Biochemistry* **1984**, *23*, 6605–6613.
(16) Eng. J. F.; Czernuszewicz, R. S.; Spiro, T. G. *J. Raman Spectrosc.* **1985**, *16*, 432–437.
(17) (a) Laane, J.; Kiefer, W. *J. Chem. Phys.* **1980**, *72*, 5305–5311. (b) Rousseau, D. L. *J. Raman Spectrosc.* **1981**, *10*, 94–99.

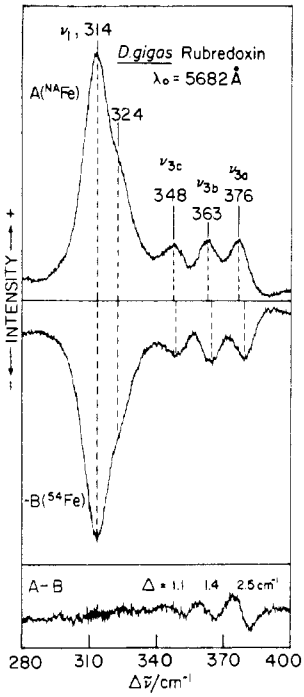

Figure 2. Resonance Raman spectra of oxidized *D. gigas* rubredoxin (A), its ^{54}Fe reconstituted protein (−B) and corresponding difference spectrum (A − B) obtained in a tuning fork difference Raman cell (liquid N_2). Both spectra were measured with 5628-Å Kr^+ laser excitation (200 mW) and 4-cm^{-2} slit widths while the spectrometer was advanced in 0.2-cm^{-1} increments. Accumulation time was 12 s/point.

are dominated by the strong band at 314 cm^{-1}, assigned to the breathing mode of the FeS_4 tetrahedron, $\nu_1(A_1)$. Two overtones of this mode can be seen, $2\nu_1$ at 627 cm^{-1} and $3\nu_1$ at 940 cm^{-1}. In the 350-cm^{-1} region, where the triply degenerate asymmetric stretch, $\nu_3(T_2)$, is expected, three bands are now clearly seen, particularly with 5682-Å excitation, at 376, 366, and 348 cm^{-1}. The 348-cm^{-1} band had previously gone undetected, and the third ν_3 component had been assigned[10] to the 324-cm^{-1} shoulder on the ν_1 band.

The ν_3 components are definitively assigned via ^{54}Fe substitution in the protein. Figure 2 shows 5682-Å-excited spectra in this region for natural abundance and ^{54}Fe–substituted proteins and the difference spectrum, obtained at low temperature with a newly designed tuning fork difference Raman cell.[16] Clear ^{54}Fe upshifts are seen for the bands at 376, 366, and 348 cm^{-1}. Analysis of the difference bands[17] gives shifts of 2.5, 1.4, and 1.1 cm^{-1}, respectively. As expected, the ν_1 band at 314 cm^{-1} does not shift (the Fe atom does not move in the breathing mode). Neither does the 324-cm^{-1} shoulder; the intensity is cancelled in the difference spectrum over the 314–324-cm^{-1} band envelope. Consequently assignment of the 324-cm^{-1} band as a component of the asymmetric Fe–S stretch is precluded. The isotope shifts for the 376-, 363-, and 348-cm^{-1} bands identify them as components of the asymmetric stretch, ν_{3a}, ν_{3b}, and ν_{3c}, the degeneracy being completely lifted.

The bending modes of the FeS_4 tetrahedron, ν_2 (E) and ν_4 (T_2), were assigned in the original work of Long and co-workers,[8] to bands at 126 and 150 cm^{-1}, respectively. Both of these bands are seen in our spectra and show a striking intensity reversal, the 150-cm^{-1} band being strongest at 5682 Å. The transition from one enhancement pattern to the other is seen with excitation at a series of Ar^+ and Kr^+ laser lines (Figure 3). Figure 4 shows the relationship of these lines to the rubredoxin absorption spectrum together with relative enhancement profiles for these modes, determined with the 230-cm^{-1} ice band as internal standard. Using 4965 Å excitation only, Yachandra et al.[10] saw only the 130-cm^{-1} band in the lower resolution solution spectrum. They also saw a weak band at 177 cm^{-1}, whereas we resolve two weak bands, at 173 and 184 cm^{-1}. These are tentatively assigned to FeSC bending modes.

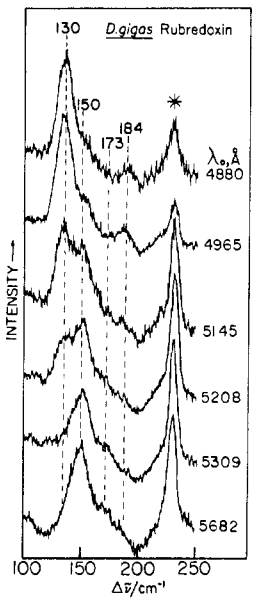

Figure 3. S–Fe–S bending region resonance Raman spectra of oxidized *D. gigas* rubredoxin obtained from frozen protein solution (liquid N_2) with various Ar^+ and Kr^+ laser excitations and 3-cm^{-1} slit widths. For these data the spectrometer was advanced in 0.5-cm^{-1} increments. An asterisk indicates the 230-cm^{-1} ice band.

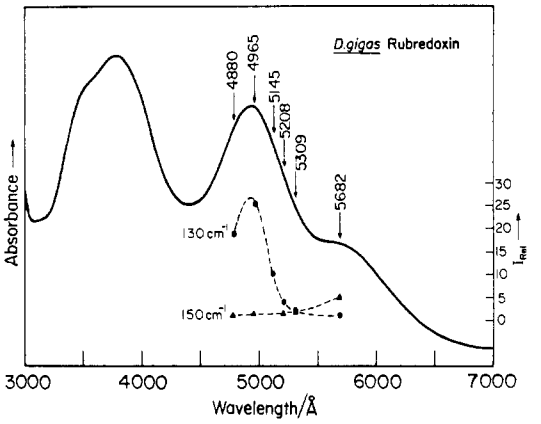

Figure 4. Relative Raman intensities (I_{rel}) profiles for S–Fe–S bending modes at 130 (●) and 150 (▲) cm^{-1} of oxidized *D. gigas* rubredoxin, superimposed on the electronic absorption spectrum. The arrows indicate various excitation wavelengths used for recording RR spectra. Raman band intensities were determined relative to the 230-cm^{-1} ice band, and normalized to the intensities at the excitation wavelengths 5682 and 4579 Å for the 130- and 150-cm^{-1} bands, respectively.

The low-temperature spectra also give much better resolution for the overtone and combination region, shown on an expanded scale in Figure 5. In addition to the prominent $2\nu_1$ overtone, bands are seen at the positions expected for the combinations $\nu_1 + \nu_2$, $\nu_1 + \nu_4$, and $\nu_1 + \nu_{3a}$, for $2\nu_{3a}$ and $\nu_{3a} + \nu_{3b}$, and even for $2\nu_1 + \nu_2$ and $2\nu_1 + \nu_4$. The band at 653 cm^{-1} does not correspond to an overtone or combination and is assigned to C–S stretching of the cysteine ligands; this is a reassignment from the 700-cm^{-1} proposal by Yachandra et al.[10] The flank of the 653-cm^{-1} band covers the region where the $\nu_1 + \nu_{3b}$ and $\nu_1 + \nu_{3c}$ combinations are expected. Qualitatively the intensities follow the expectation from scattering theory[18] that the overtone and combination band intensity should scale as the squares and the products of the intensities of the fundamental modes. No anomalous intensities are seen as in the case of the "blue" copper proteins.[19,20]

(18) Heller, E. J.; Sundberg, R. L.; Taunor, D. *J. Phys. Chem.* **1982**, *86*, 1822–1833.
(19) Blair, D. F.; Campbell, G. W.; Schoonover, J. R.; Chan, S. I.; Gray, H. B.; Malmstrom, B. G.; Pecht, I.; Swanson, B. I.; Woodruff, W. H.; Cho, W. K.; English, A. M.; Fry, H. A.;f Lum, V.; Norton, K. A. *J. Am. Chem. Soc.* **1985**, *107*, 5755–5766.

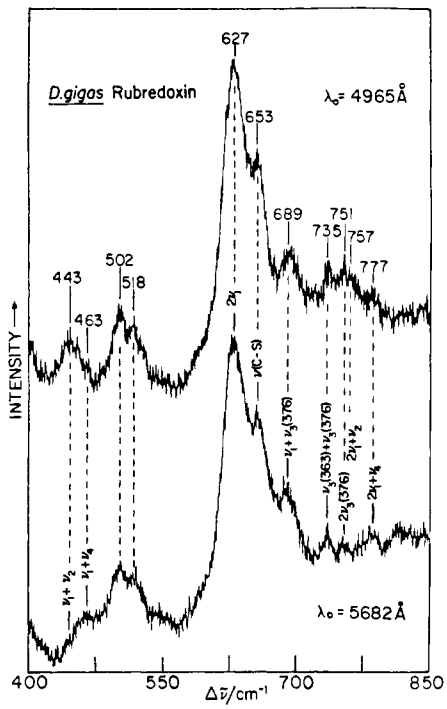

Figure 5. Low-temperature Fe–S overtone region resonance Raman spectra of oxidized *D. gigas* rubredoxin obtained with 4965-Å Ar^+ (upper trace) and 5682-Å Kr^+ (lower trace) laser excitations and 8-cm^{-1} slit widths. For these data the spectrometer was advanced in 0.5-cm^{-1} increments.

Discussion

Fe–S Modes: Isotope Shifts and Coupling to Protein Modes. In the absence of vibrational coupling between the FeS_4 tetrahedron and the protein, the lifting of the ν_3 degeneracy would have to result from angular distortions, since the Fe–S bonds are equal in length.[3,5] In the *C. pasteurianum* rubredoxin crystal structure[3] the S–Fe–S angles deviate modestly from the tetrahedral value, 109.5°; they range from 114.3 to 103.8°. Trial calculations by Yachandra et al.[10] showed that this variation could produce a splitting of ~15 cm^{-1}. This is not insignificant, but is only half of the spread between ν_{3a} and ν_{3c}.

Some coupling with other modes is clearly indicated, however, by the isotope shifts of the ν_3 components. The 2.5-cm^{-1} shift for the ν_{3a} mode is close to that expected[24] for ν_3 of an isolated FeS_4 tetrahedron, but the 1.4- and 1.1-cm^{-1} shifts of ν_{3b} and ν_{3c} are significantly lower. The missing isotope shifts must be associated with other modes, with which ν_{3b} and ν_{3c} are coupled. The likeliest candidate for coupling is the SCC bending mode, which interacts strongly with Fe–S stretching when the two internal coordinates are in line, i.e. when the Fe–S–C–C dihedral angle is 0 or 180°. Yachandra et al.[10] carried out normal mode calculations on a $Fe(SCH_2CH_3)_4$ model and showed that the pronounced difference in the ν_1 frequency of rubredoxin and the analogue $Fe(S_2\text{-}o\text{-}xyl)_2^-$, 312 vs. 297 cm^{-1}, could be accounted for by the differing Fe–S–C–C dihedral angles; in $Fe(S_2\text{-}o\text{-}xyl)_2^-$ they are all ~90°,[6] uncoupled from the Fe–S stretches, whereas in rubredoxin two of them are ~90° while the other two are ~180°.[3] The δ_{SCC} frequency itself was calculated to be ~290 cm^{-1}. We have extended these calculations and find that the reduction in the ^{54}Fe isotope shifts for ν_{3b} and ν_{3c} requires δ_{SCC} to be somewhat higher, ~320 cm^{-1}. It is therefore plausible that the 324-cm^{-1} shoulder in the rubredoxin spectra is assignable to δ_{SCC}. Although some ^{54}Fe sensitivity is predicted for this mode via the coupling with ν_{3b} and ν_{3c}, it might be too small to be detected in the difference spectrum, especially since most of the intensity in this region is provided by the 314-cm^{-1} ν_1 band. A ν_3 splitting of at least 20 cm^{-1} is readily provided by coupling to δ_{SCC},[10] so that the spread of ν_3 component frequencies can be accounted for by a combination of angle distortion and vibrational coupling.

Wavelength Dependence and Symmetry: Vibronic Coupling. The striking intensity reversal of the S–Fe–S bending modes when the excitation wavelength is varied from 4880 to 5682 Å (Figures 3 and 4) results from different enhancement mechanisms for the two modes. The electronic absorption spectrum has been assigned via single-crystal polarization measurements by Eaton and Lovenberg.[2] Two major absorption bands are seen in the visible and near-UV region (Figure 4), at 495 and 380 nm, attributable to charge transfer from sulfur to the $d_\pi(e)$ and $d_\sigma(t_2)$ orbitals on Fe^{III}. The allowed transitions are of T_2 symmetry in the T_d point group, but the prominent shoulders seen on both of the absorption bands imply a significant reduction in symmetry. Eaton and Lovenberg found an axial distoriton to be sufficient to account for the spectra (the rhombic splitting was estimated to be less than half the axial splitting) and located the distortion axis almost along the S_4 axis of the FeS_4 tetrahedron, giving an effective excited-state symmetry of D_{2d}.[2] The 495-nm band and its 565-nm shoulder were assigned respectively to the ^6E and $^6D_2$ components of the lower $^6T_2$ charge-transfer state, the ground state being $^6A_1$.

In D_{2d} symmetry, the T_2 vibrations have E and B_2 components while the E vibrations have A_1 and B_1 components. Although the RR spectra were obtained on frozen solutions, which tend to depolarize the scattered light via multiple reflections, we found the spectra to be partially polarized, due to the diminution of multiple scattering in the highly absorbing samples.[21,15] The 130-cm^{-1} band was clearly more polarized than the 150-cm^{-1} band. This observation leads us to assign the 130-cm^{-1} band to the A_1 (totally symmetric in D_{2d} symmetry) component of the ν_2(E) vibration. It is enhanced via the strong 495-nm transition, presumably via A term[22] (Franck–Condon) scattering, which favors totally symmetric modes along which the excited state is displaced.[23] In contrast the 150-cm^{-1} band is enhanced via the weaker 565-nm transition, and since it appears to be depolarized, we attribute the enhancement to a B term[22] (vibronic) mechanism, whereby the vibration in question is effective in mixing the local excitation with a nearby stronger one.[23] If the 565-nm transition is vibrationally mixed with the stronger 495-nm transition, the symmetry of the coupling modes must be $B_2 \times E = E$. For this reason we assign the 150-cm^{-1} band to the E component of the $\nu_4(T_2)$ vibration. The separate components of the ν_2 and ν_4 vibrations need not differ significantly in frequency. The frequency separation depends on the ground-state distortion, whereas the intensities and enhancement mechanisms are determined by distortions in the excited states. It is interesting that the weak 184-cm^{-1} band is enhanced via the 495-nm transition while the 173-cm^{-1} band is enhanced via the 565-nm transition (see Figure 3). These bands are tentatively assigned to Fe–S–C bending modes, but they no doubt couple strongly with the S–Fe–S bends and acquire similar symmetry properties.

It is also of interest that the bands assigned to ν_{3b} and ν_{3c} gain intensity relative to ν_{3a} at 5682 Å (see Figure 1). This suggests that these two bands have E character in the D_{2d} electronic symmetry. The effective ground-state symmetry pertinent to these modes must of course be lower than D_{2d} symmetry to account for the complete removal of the ν_3 degeneracy. Nevertheless, the enhancement pattern suggests that ν_{3b} and ν_{3c} belong to modes that are polarized perpendicular to the S_4 axis (E), while ν_{3a} is

(20) Nestor, L.; Reinhammar, B.; Spiro, T. G., submitted for publication in *Biochim. Biophys. Acta.*

(21) (a) Strommen, D. P.; Bajdor, K.; Czernuszewicz, R. S.; Blinn, E. L.; Nakamoto, K. *Inorg. Chim. Acta* **1982**, *63*, 151–155. (b) Spaulding, L. D.; Change, C. C.; Yu, N.-T.; Felton, R. H. *J. Am. Chem. Soc.* **1975**, *97*, 2517–2525.

(22) (a) Albrecht, A. C. *J. Chem. Phys.* **1961**, *34*, 1476–1484. (b) Tang, J.; Albrecht, A. C. *J. Chem. Phys.* **1968**, *49*, 1144–1154.

(23) Spiro, T. G.; Stein, P. *Ann. Rev. Phys. Chem.* **1977**, *28*, 501–521.

(24) Urey–Bradley force constants, $K_{Fe\text{-}S}$ = 1.30 mdyn/Å, $H_{S\text{-}Fe\text{-}S}$ = 0.30 mdyn/Å, and $F_{S\cdots S}$ = 0.14 mdyn/Å transferred from ref 10, produced the following frequencies for a tetrahedral FeS_4 molecule: $\nu_1(A_1)$ = 314 cm^{-1}; $\nu_3(T_2)$ = 363 cm^{-1}; $\nu_4(T_2)$ = 150 cm^{-1}; $\nu_2(E)$ = 134 cm^{-1}. The ^{54}Fe natural-abundance isotopic shift for the 363 cm^{-1} frequency was then calculated to be 2.7 cm^{-1}.

polarized parallel to it (B_2). This identification of the eigenvectors may prove helpful in unravelling the vibrational couplings that determine the frequencies and isotope shifts of the bands.

Conclusions

(1) ^{54}Fe isotope shifts lead to definitive assignments of the ν_3 asymmetric stretching vibration of the FeS_4 tetrahedron, which is split into components at 376, 363, and 348 cm^{-1}. The lower than expected isotope shifts for the latter two established that they are coupled to protein vibrational modes, probably involving SCC bending in the cysteine ligands. The 324-cm^{-1} shoulder on the 314-cm^{-1} ν_1 band is tentatively assigned to a δ_{SCC} band.

(2) Variable-excitation and depolarization measurements provide assignments for the A_1 and E components of the ν_2 and ν_4 modes; the latter can mix the B_2 and E components of the lower energy ($S_\pi \rightarrow Fe_{d\pi}$) charge-transfer transition. A similar enhancement pattern identifies the lower two ν_3 bands, at 363 and 348 cm^{-1}, with the perpendicular (E) components of the asymmetric stretch.

(3) Numerous overtone and combination bands are observed in the frozen-solution spectra, with normal intensity patterns. A band at 653 cm^{-1} is assigned to S–C stretching of the cysteine ligand.

The assignments are detailed in Table I.

Acknowledgment. This work was supported by NIH Grant GM 13498.

Registry No. ^{54}Fe, 13982-24-6; ^{56}Fe, 14093-02-8.

Contribution from the Department of Applied Chemistry, Faculty of Engineering, Yamanashi University, Takeda, Kofu 400, Japan, and Electrotechnical Laboratory, Sakura-mura, Niihari-gun, Ibaraki 305, Japan

EXAFS Study of Chromium Ions in the Mixed-Solvent System of Formamide and Ammonium Formate

Michihiro Miyake,*† Nobuhiro Nakagawa,†§ Hiroyuki Ohyanagi,‡ and Takashi Suzuki†

Received February 20, 1985

EXAFS (extended X-ray absorption fine structure) spectra of Cr ions exhibiting two oxidation states, Cr(VI) and Cr(III), in the mixed-solvent system of $HCONH_2$ and $HCOONH_4$ have been investigated for the Cr K edge by Fourier transform and parameter-fitting methods. In the mixed-solvent system, it was found that Cr(VI) ions form mononuclear CrO_4^{2-} tetrahedra with Cr–O bond lengths of 1.61 Å and Cr(III) ions form mononuclear $[Cr(HCOO)_x(HCONH_2)_y]^{3-x}$ ($x + y = 6$; $4 \le x \le 6$) octahedra with Cr–O bond lengths of 2.00 Å. The CrO_4^{2-} tetrahedra, which exist in the mixed-solvent system at an initial state of dissolution of CrO_3, are transformed into the $[Cr(HCOO)_x(HCONH_2)_y]^{3-x}$ octahedra by heating reduction.

Introduction

Ammonium formate ($HCOONH_4$), which has been found to be a molten salt with low melting point (mp 116 °C),[1] is partially decomposed into formamide ($HCONH_2$) and water although molten $HCOONH_4$ can dissolve various metallic oxides that are insoluble in water. The mixed-solvent system of $HCONH_2$ and $HCOONH_4$, therefore, has been utilized as the model solvent of the molten $HCOONH_4$ bath. The dissolution characteristics of metallic oxides in the $HCONH_2 + HCOONH_4$ system have been investigated on the basis of visible absorption spectra and ESR spectra, and this mixed-solvent system was found to have outstanding properties as a metal-plating bath.[1-4] Though the structure of liquid $HCONH_2$ was analyzed by X-ray diffraction,[5,6] the coordination structure of metallic ions in the $HCONH_2 + HCOONH_4$ system has been unexplained.

The Cr atoms exhibit two oxidation states, Cr(VI) and Cr(III), in the $HCONH_2 + HCOONH_4$ system, and a blackish corrosion-resistant chromium film can be successfully electrodeposited on the condition that there exist Cr(III) ions in this bath.[2] It is of interest to compare the coordination structure of Cr(III) ions with that of Cr(VI) ions in the $HCONH_2 + HCOONH_4$ system to aid in elucidating the mechanism of electrodeposition from this bath.

In this paper, we describe the results obtained by EXAFS (extended X-ray absorption fine structure) experiments of Cr(VI) and Cr(III) ions in the $HCONH_2 + HCOONH_4$ system for the Cr K edge. The coordination structures of the Cr(VI) and Cr(III) ions are demonstrated on the basis of the experimental results, associated with previous results.[1,2]

Experimental Section

Sample I, which was a brown solution, was prepared by dissolving 3.2 g (0.03 mol) of CrO_3 and 25 g (0.4 mol) of $HCOONH_4$ in 100 cm^3 of $HCONH_2$ at room temperature. Sample II, which was a purple solution, was prepared by reducing sample I with stirring at about 90 °C for 36 h. The visible absorption spectra of these solutions were measured to clarify the oxidation state of the Cr ions.

The solution was contained in an aluminum cell with Kapton (30 μm) windows through which X-rays were passed, and the thickness of the cell was adjusted in order to get the optimum absorption jump at the Cr K edge. Reference compounds such as K_2CrO_4 and Cr_2O_3 crystals were chosen, considering the oxidation states of the Cr ions in the solutions. Cr(VI) ions are tetrahedrally surrounded by four O atoms in the K_2CrO_4 crystal belonging to K_2SO_4 type, and Cr(III) ions are octahedrally surrounded by six O atoms in Cr_2O_3 crystals belonging to corundum type. Crystals were ground into fine powders and sandwiched between adhesive tapes. Special care was taken to produce homogeneous films to avoid distortion in the spectra.

The X-ray absorption spectra have been measured on the EXAFS apparatus[7,8] installed at BL 10B in the Photon Factory of the National Laboratory for High Energy Physics (KEK). The synchrotron radiation, running typically at 2.5 GeV with the beam current in the range 70–150 mA, was monochromated with a silicon (311) channel-cut crystal under helium gas. Intensities were monitored by two ionization chambers (I_0 and I) filled with N_2 and Ar gases, respectively. The spectral range covered was 1300 eV, of which 300 eV was preedge, and an energy resolution of 1.7 eV with a photon flux of 10^8–10^9 photons/s was achieved in the vicinity of the Cr K edge (5.989 keV).

Results and Discussion

The visible absorption spectra for solutions I and II are shown in Figure 1. The maxima at about 410 nm for solution I and

† Yamanashi University.
‡ Electrotechnical Laboratory.
§ Present address: Shin-etsu Chemical Co., Gunma, Japan.

(1) Suzuki, T.; Hayakawa, Y. *Molten Salts* **1976**, *19*, 127.
(2) Suzuki, T.; Hatsushika, T.; Hayakawa, Y. *Molten Salts* **1980**, *23*, 135.
(3) Suzuki, T.; Hatsushika, T.; Hayakawa, Y. *Nippon Kagaku Kaishi* **1982**, 1017.
(4) Hayakawa, Y.; Hatsushika, T.; Suzuki, T. *Denki Kagaku oyobi Kagyo Butsuri Kagaku* **1983**, *51*, 203.
(5) Ohtaki, H.; Funaki, A.; Rode, B. M.; Reibnegger, G. J. *Bull. Chem. Soc. Jpn.* **1983**, *56*, 2116.
(6) Miyake, M.; Kaji, O.; Nakagawa, N.; Suzuki, T. *J. Chem. Soc., Faraday Trans. 2* **1985**, *81*, 277.
(7) Photon Factory Activity Report of the National Laboratory for High Energy Physics, Japan, 1982/1983; V-28.
(8) Ohyanagi, H.; Matsushita, T. *Kotai Butsuri* **1983**, *18*, 515.

0020-1669/86/1325-0700$01.50/0